



Deformation behaviors of various Fe–Mn–C twinning-induced plasticity steels: effect of stacking fault energy and chemical composition

Joong-Ki Hwang^{1,*}

¹ School of Mechanical Engineering, Tongmyong University, Busan 48520, Republic of Korea

Received: 13 June 2019

Accepted: 10 September 2019

Published online:

17 September 2019

© Springer Science+Business Media, LLC, part of Springer Nature 2019

ABSTRACT

Tensile behaviors of the 14 high-manganese steels having stacking fault energy (SFE) range of 13–41 mJ/m² using different C, Mn, Cu, Al, and Si contents have been investigated to find a general relationship between SFE and tensile properties in Fe–Mn–C TWIP steels. Cu and Al played similar roles in TWIP steels; however, the effect of Al content was much higher than that of Cu content. Addition of C and Si highly increased the yield strength, but excessive additions led to the premature and early fracture, respectively. The serration flow in tensile curve was not observed when the ratio of Al to C is over about 3.0, which means the critical ratio of Al to C to eliminate the serration flow in high-manganese steels was in existence. Dynamic strain aging decreased the post-necking elongation during tensile test associated with the premature fracture, leading to the decrease in reduction of area (RA) in TWIP steels. It was found that most of the tensile properties such as yield strength, tensile strength, and elongations had no relationship with SFE; however, RA had a relatively higher relationship with SFE, which means RA is a potential indicator to evaluate SFE and twinning behavior in Fe–Mn–C high-manganese steels. Also, twinning stress had a linear relationship with SFE in TWIP steels and Schmid factor of 0.5 was needed to use for polycrystalline metals to evaluate the twinning stress using the models based on the single crystal.

Introduction

With the increased demands for high-strength materials in automotive industries, twinning-induced plasticity (TWIP) steels have attracted much interest as a novel type of advanced high-strength automotive steels over the past few decades due to their

excellent combination of strength and ductility stemming from the deformation twins and/or dynamic strain aging (DSA) during plastic deformation [1–7]. Most of the previous studies have attributed the outstanding tensile properties of TWIP steels to deformation twin because fine deformation twins formed during plastic deformation reduce the

Address correspondence to E-mail: jkhwang@tu.ac.kr

effective grain size of steels. It is well known that the mechanism of twin formation is strongly affected by the stacking fault energy (SFE). Allain et al. [8] proposed that deformation twinning is activated when the SFE is between 12 and 35 mJ/m², whereas ϵ -martensite transformation occurs when the SFE is lower than 18 mJ/m². Saeed-Akbari et al. [9] reported a SFE of 20 mJ/m² as the upper limit for ϵ -martensite transformation, whereas Kim and De Cooman [10] reported that the upper limit of SFE value for ϵ -martensite transformation is approximately 13 mJ/m². Curtze and Kuokkala [11] reported that plasticity and strain hardening are mainly related to the perfect dislocation when the SFE is higher than 45 mJ/m². Moreover, Park et al. [12] proposed a new plasticity mechanism in high-manganese steels having SFE of around 80 mJ/m² called microband-induced plasticity (MBIP) in which microbands were formed by dislocation planar gliding. Overall, it is possible to conclude that TWIP effect was strong in the SFE range from 20 to 40 mJ/m² although these limits are not immovable. It is well accepted that the SFE is mainly controlled by chemical composition and deformation temperature [9–11, 13–17].

Meanwhile, DSA, commonly explained as results of the dynamic interaction of solute interstitial atoms and dislocations during plastic deformation, typically occurs in C-added TWIP steels. The DSA effect on the strain hardening rate in TWIP steels is still debated. It is generally known that DSA had limited contribution to strain hardening rate in TWIP steels in comparison with the deformation twinning [18, 19]. In contrast, Shun et al. [20] and Dastur and Leslie [4] suggested that DSA had a major contribution to strain hardening rate in TWIP steels, and Zhou and Huang [21] reported that the contribution of DSA on the strain hardening rate is only significant at the beginning stage of deformation. In the fields of manufacturing industry, the Portevin–Le Chatelier (PLC) effect induced by DSA is one of the crucial issues since serrated flow can make not only strain marks on the surface of products but also cracks during the forming process [22].

Despite the outstanding combination of strength and ductility, TWIP steels have some crucial problems such as difficulties in steelmaking process in industrial scale due to high Mn contents [23] and relatively low yield stress (YS), which limited the commercialization of TWIP steels. Accordingly, many efforts to overcome the technical difficulties

stemming from the high Mn addition in mass production scale have been conducted using other various alloy elements such as Al, Cu, N, and C to reduce Mn addition [16, 23–33]. Al, Cu, N, and C stabilize austenite and inhibit martensite transformation by increasing the SFE; thus, they can replace or reduce Mn content in TWIP steels. Meanwhile, several researchers have investigated the effects on the process designs as well as alloy designs in high-manganese steels to increase the mechanical properties, especially YS. They increased mechanical properties of steels by optimizing the rolling temperature [34, 35], strain rate [36], pre-stain [37, 38], and addition of alloys such as Si [39, 40], C [41], Al [25], and V [42].

Therefore, from scientific and industrial point of view, understanding and predicting the deformation behaviors of TWIP steels with SFE and alloy elements is becoming increasingly significant. It was reported that Al additions increase the YS due to solid solution hardening and decrease the strain hardening rate or tensile stress (TS) due to the suppression of twin formation during plastic deformation [23, 25, 29]. The Cu additions increase the total elongation (TE) without a slight loss of TS [16, 26]. Liu et al. [33] and Kusakin et al. [41] reported that the YS increased with an increase in C content in Fe–Mn–C–Al TWIP steels. Lee et al. [39] reported that the addition of Si to Fe–18Mn–0.6C (wt%) TWIP steel triggered deformation twinning earlier due to the reduction of SFE and increased the YS due to the solid solution hardening.

Although there have been many studies on the effects of SFE and chemical compositions on tensile properties of TWIP steels, most of the studies have been conducted qualitatively or fragmentarily, and few articles have been reported on the effect of SFE on tensile properties comprehensively [10]. Moreover, no articles have been found on the direct relationship between SFE and tensile properties in TWIP steels. These results of the literature reviews stimulated an additional investigation on the behaviors of tensile properties with the extensive changes in the chemical compositions or SFE. The present study, therefore, deals with the influence of SFE on the tensile properties of TWIP steels to understand and predict the tensile behavior with SFE. Also, the effect of chemical compositions on tensile properties is broadly compared to elucidate the role of chemical compositions comprehensively. Furthermore, the twinning stress was evaluated using electron

backscatter diffraction (EBSD) techniques. To achieve the above aims, 14 high-manganese steels with a systemic variation of C, Mn, Cu, Al, and Si contents were prepared in the same process and tested in the same manner to reduce the influence of other factors except for SFE and/or chemical composition.

Experimental

The 50-kg ingots of 14 high-manganese steels with different C, Mn, Cu, Si, and Al contents were prepared by vacuum induction melting. Table 1 summarizes their analyzed chemical compositions. For convenience, these steels are referred to as the name and group described in Table 1. The cast ingots of 125 mm in thickness were homogenized at 1200 °C for 12 h to avoid the segregation of alloy elements and subsequently hot-rolled to a 20-mm-thick plates (an average thickness reduction per pass of 20%) without intermediate reheating at temperature ranging from 950 to 1150 °C, followed by air cooling to room temperature. The microstructures of the group 1 consist of fully recrystallized grains with an average grain size of 38–45 μm [43] except for the 3.0Si steel. The average grain size of the 3.0Si steel was 81 μm stemming from the high Si content. And the group 2 may have a grain size range of 25–30 μm [44] although all the steels were not characterized in detail.

The calculated SFEs of the present steels based on thermodynamic model of Saeed-Akbari et al. [9] and

Dumay et al. [14] are in the range of 13–41 mJ/m² as shown in Table 1. Olson and Cohen [45] and Adler et al. [46] suggested the following equation to calculate the SFE of FCC structures:

$$\Gamma = 2\rho G^{\gamma \rightarrow \varepsilon} + 2\sigma^{\gamma/\varepsilon}, \tag{1}$$

where Γ , ρ , $G^{\gamma \rightarrow \varepsilon}$, and $\sigma^{\gamma/\varepsilon}$ refer to SFE, molar surface density, free energy for $\gamma \rightarrow \varepsilon$ phase transformation, and γ/ε interfacial energy, respectively. Saeed-Akbari et al. [9] calculated the SFE considering the grain size effect by adding a modified term based on the existing thermodynamic model as follows:

$$\Gamma_{\text{eff}} = \Gamma + 2\rho \Delta G_{\text{ex}} = \Gamma + \Gamma_{\text{ex}}, \tag{2}$$

where Γ_{eff} , ΔG_{ex} , and Γ_{ex} mean effective SFE, excess free energy with grain size effect, and excessive SFE with grain size effect, respectively. The Γ_{ex} can be represented as the following equation [47]:

$$\Gamma_{\text{ex}} = 2\rho \Delta G_{\text{ex}} = 2\rho \left[170.06 \exp\left(-\frac{D}{18.55}\right) \right]. \tag{3}$$

The differences Γ and Γ_{eff} were small in this study due to the grain size range of 25–45 μm [17].

Round-type tensile specimens (gauge diameter of 5 mm and length of 25 mm) were prepared along the axis parallel to the hot-rolling direction. They were tested at room temperature at an initial strain rate of 10⁻³ s⁻¹ using an Instron machine equipped with a mechanical extensometer. For each steel grade, at least three specimens were tested and the average value was reported. Reduction of area (RA) or the minimum reduced diameter value was carefully

Table 1 Analyzed chemical composition and calculated SFE of the investigated 14 high-manganese steels with various C, Mn, Cu, Al, and Si contents

Group	Steel	Chemical composition (wt%)						SFE (mJ/m ²)		Comments
		C	Mn	Cu	Al	Si	Fe	Γ	Γ_{eff}	
Group 1	0CuAlSi	0.71	16.63	–	–	–	Bal.	16.0	17.2	Base
	1.5Cu	0.72	16.94	1.52	–	–	Bal.	18.9	20.1	Cu effect
	3.0Cu	0.72	17.07	2.90	–	–	Bal.	21.1	22.3	Cu effect
	1.5Al	0.70	17.18	–	1.50	–	Bal.	30.0	31.2	Al effect
	3.0Al	0.69	17.26	–	2.80	–	Bal.	39.0	40.3	Al effect
	1.5Si	0.69	17.08	–	–	1.48	Bal.	14.5	15.5	Si effect
	3.0Si	0.70	17.19	–	–	2.90	Bal.	13.5	13.6	Si effect
Group 2	20Mn0.6C1Al	0.60	19.94	–	1.03	–	Bal.	21.4	23.5	Base
	0.3C	0.30	20.0	–	1.03	–	Bal.	13.3	15.3	C effect
	0.9C	0.91	19.9	–	1.02	–	Bal.	29.5	31.6	C effect
	15Mn	0.61	15.02	–	1.01	–	Bal.	15.7	17.8	Mn effect
	25Mn	0.59	24.76	–	0.99	–	Bal.	28.2	30.3	Mn effect
	0Al	0.61	19.81	–	–	–	Bal.	14.7	16.8	Al effect
	2Al	0.6	20.59	–	1.92	–	Bal.	28.0	30.1	Al effect

measured with the well-designed magnifier after the tensile test.

The twinning behaviors were analyzed by EBSD techniques on the cross section of samples perpendicular to the tensile axis. Samples for EBSD measurement were carefully prepared by mechanical polishing down to 1 μm using diamond pastes followed by a colloidal silica slurry polisher. EBSD data were taken using a FE SEM equipped with a TSL EBSD system at a sample tilt angle of about 70° under 20 keV. All the acquired EBSD data were interpreted by the orientation imaging microscopy (OIM) analysis commercial software provided by TexSEM Laboratories.

Results and discussion

Mechanical properties

The representative engineering stress–strain curves and TE–TS balance map of the 14 high-manganese steels are displayed in Figs. 1 and 2, and average tensile properties are summarized in Table 2. They were categorized as two groups according to the base chemical composition: nominal composition of Fe–17Mn–0.7C in group 1 and Fe–20Mn–0.6C–1Al in group 2. All the steels except for the 3.0Si steel exhibited an excellent combination of high strength and large elongation, low YS, and small post-necking elongation (PE), which are typical characteristics of TWIP steels [3, 25]. The YS increased with increasing Al, Cu, C, and Si content as shown in Fig. 3, which can be explained by the solid solution strengthening effect of these alloy elements in austenite matrix. Carbon additions dramatically increased the YS in Fe–Mn–C TWIP steels [33, 41], i.e., about 216 MPa per one weight percent. And Si, Al, and Cu increased the YS [16, 25, 39] of 38, 18, and 4 MPa per one weight percent, respectively. The influence of Mn addition on YS was very small. It is worth noting that the influence of Si addition on the solid solution strengthening was higher than that of Al and Cu additions.

The TS was decreased with the addition of Cu, Al, and Mn elements and increased with C content as shown in Figs. 1d and 2d, which was well reported by many researchers [10, 16, 25, 26, 29, 41]. Compared to the effect of Al addition showing the decrease in TS and TE, the addition of Cu content not only

represented a relatively small decrease in TS but also exhibited an increase in TE (Fig. 1d). Meanwhile, it was reported that TWIP steels with Cu additions had a higher resistance to delayed fracture compared to Fe–Mn–C TWIP steels [48, 49]. The commercialization of TWIP steels is also delayed by Al addition as well as Mn addition, e.g., nozzle blocking during the continuous casting process in industrial scale. Accordingly, the author cautiously suggests that Cu-added TWIP steels can replace Al-added TWIP steels and reduce Mn contents in TWIP steels.

The behavior of elongation was very complex with chemical compositions, and it is difficult to find a reasonable trend, which will be discussed later part. RA value increased with increasing Al, Cu, and Mn, whereas it decreased with increasing C as summarized in Table 2. Unexpectedly, all the specimens of the 3.0Si steel were fractured during the tensile test as shown in Fig. 1c since the main deformation mode may change from deformation twin to ϵ -martensite transformation stemming from the low SFE of 13.6 mJ/m^2 [39, 50].

The variations in tensile properties with effective SFE (Γ_{eff}) of the 13 steels are represented in Fig. 4 to investigate the relationship between SFE and tensile properties. The 3.0Si steel was excluded in this comparison due to the earlier fracture. Although YS increased roughly with increasing SFE, the reasonable dependence of strength and SFE was hardly observed (Fig. 4a) since YS was strongly dependent on the chemical composition itself (Figs. 1, 2, 3) rather than SFE. For instance, the YS increased by the solid solution hardening effect of C, Al, and Cu, which also increased the SFE, whereas YS increased with the addition of Si (Fig. 3), which decreased the SFE. In fact, the effect of the SFE can be appreciable only after the onset of plastic deformation since the stability or metastability of the austenite is only appreciable after yielding. Especially in TWIP steels, twinning behaviors are highly dependent on the SFE, which means the effect of SFE appeared after plastic deformation.

The TS decreased roughly with increasing SFE since twinning rate tends to decrease with increasing SFE in the SFE range of occurring TWIP effect, resulting in decreasing the strain hardening rate [25]. However, the deviations of measured data from the linear fitting line were too big (Fig. 4a) because TS was dependent on the several complex factors such as YS, twinning rate, DSA effect, and strain hardening rate. The TE also did not show a reasonable

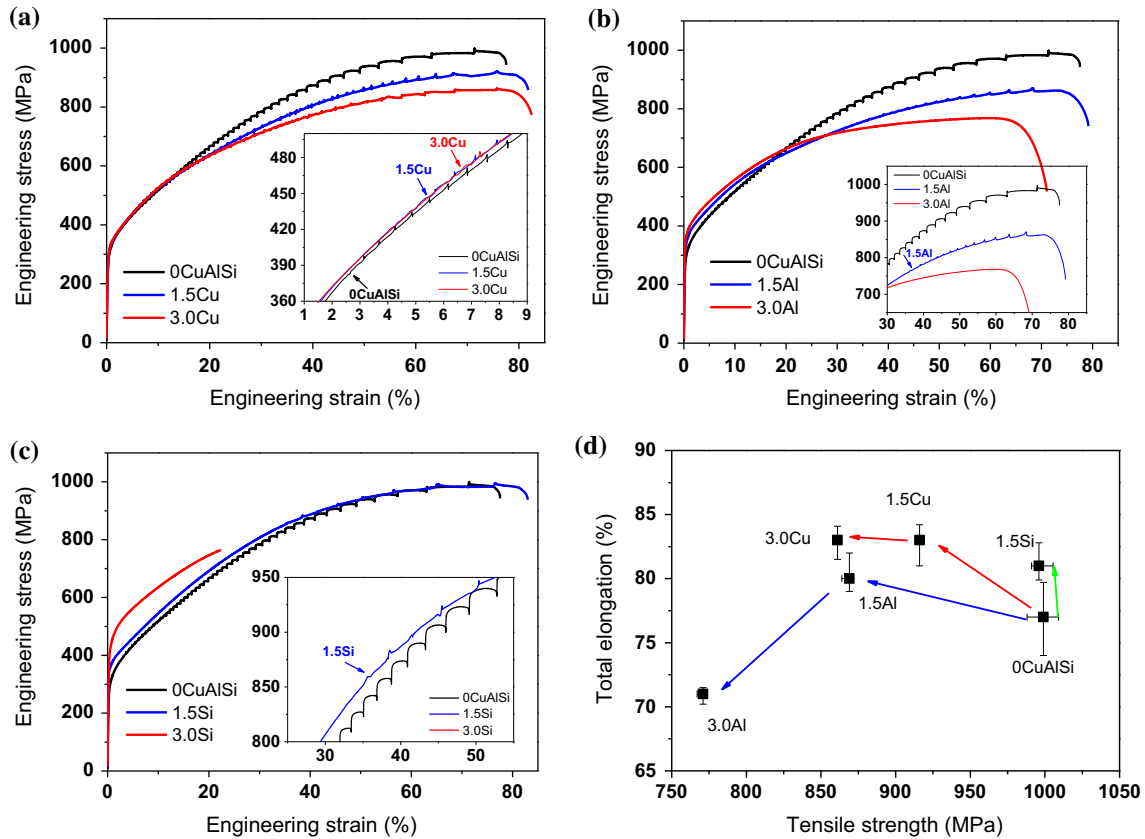


Figure 1 Engineering stress–strain curves with variation of chemical composition: **a** Cu effect, **b** Al effect, and **c** Si effect, and **d** influence of chemical composition on tensile properties of the six steels (group 1).

relationship with the SFE (Fig. 4b). Consequently, ECO index, the product of TS and TE, had no relationship with SFE although ECO index was roughly decreased with increasing SFE (Fig. 4c). These rough trends of decrease in TS, TE, and ECO index with increasing SFE were related to the twinning behaviors since the lower SFE activates deformation twinning within the SFE range of twin dominant plastic deformation region.

More interestingly, the RA value was found to be closely related to the SFE as shown in Fig. 4d: RA values increased almost linearly with increasing SFE. The PE also had a linear relationship with SFE. It should be noted that the large deviation of the 0.9C TWIP steel from this linear relationship can be due to the premature fracture of tensile specimen stemming from the active DSA. In TWIP steels, PE value can mainly reflect the DSA behavior. The relationship between SFE and RA will be discussed in the next section. Meanwhile, the trend of RA and TE was found to be opposite with SFE although both values are the well-known ductility parameters. In the case

of TWIP steels, TE is highly dependent on the uniform elongation (UE) because PE is relatively small compared to UE; therefore, TE was decreased with increasing SFE due to the suppression of TWIP effect in larger SFE range as shown in Fig. 4b. On the other hands, RA strongly depends on the PE rather than UE. As shown in Fig. 4d, PE increased with SFE, resulting in increasing RA with increasing SFE.

DSA and RA in TWIP steels

Except for 3.0Al, 2Al, and 0.3C steels, the flow curves exhibited significant serrations resulting from the so-called PLC or DSA effect [4, 21, 51–53] as shown in Figs. 1 and 2. The smaller box in Figs. 1 and 2 displays the enlargement of stress–strain curve to observe the critical strain or stress for the onset of serration. When the difference in between higher stress and lower stress was over than 3 MPa in the tensile curve, it was defined as the onset strain of serration. Serrations were not observed in the tensile curves of 3.0Al and 2Al steels. Jin et al. [25] suggested

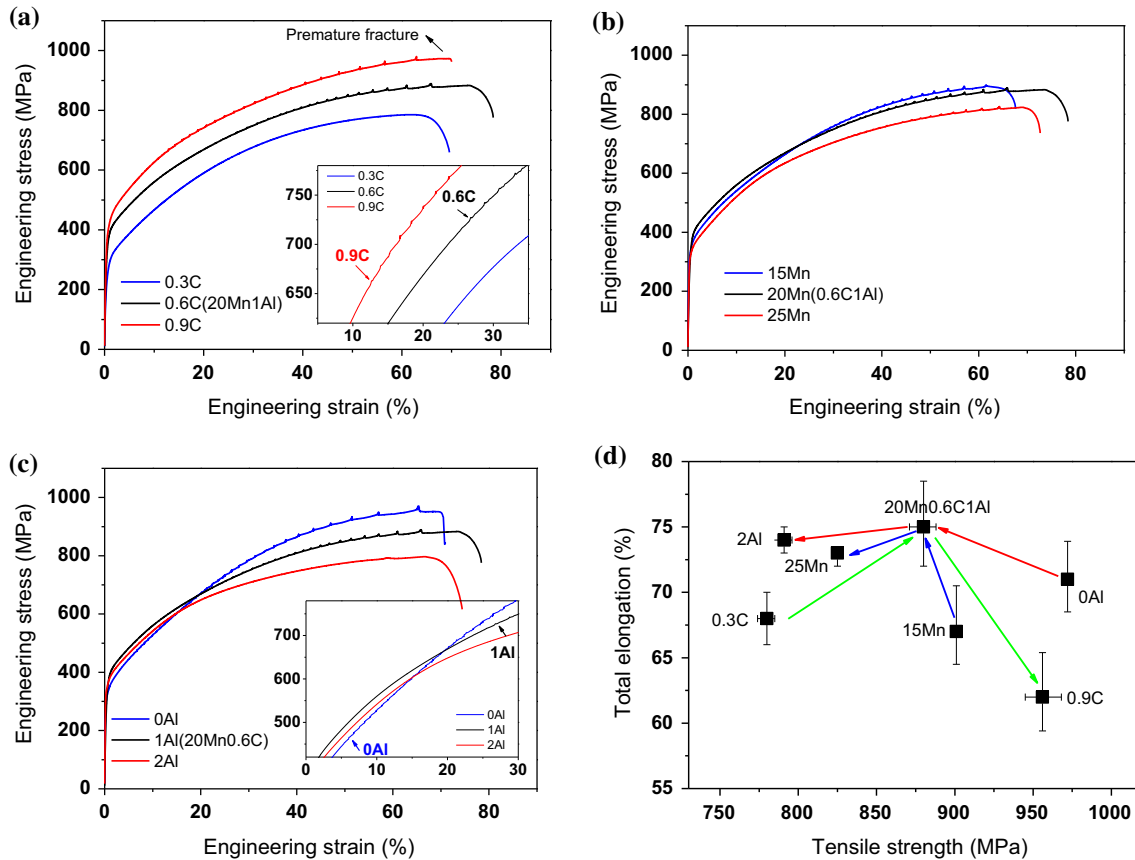


Figure 2 Engineering stress–strain curves with variation of chemical composition: **a** C effect, **b** Mn effect, and **c** Al effect, and **d** influence of chemical composition on tensile properties of the seven steels (group 2).

Table 2 Average tensile properties of the 14 high-manganese steels used in the present study

Group	Steel	YS (MPa)	TS (MPa)	TE (%)	RA (%)	Onset of serration	
						Strain	Stress (MPa)
Group 1	0CuAlSi	294	999	77	54	2.7	384
	1.5Cu	297	916	83	57	4.3	422
	3.0Cu	311	861	83	63	6.3	462
	1.5Al	329	869	80	66	37	766
	3.0Al	365	771	71	77	None	None
	1.5Si	354	996	81	56	36	859
	3.0Si	403	–	–	–	–	–
Group 2	20Mn0.6C1Al	325	880	75	63	27	727
	0.3C	225	780	68	59	None	None
	0.9C	354	956	62	55	13	666
	15Mn	321	901	67	56	27	735
	25Mn	313	825	73	65	35	734
	0Al	310	972	71	60	6.6	473
	2Al	333	791	74	68	None	None

YS yield strength, TS tensile strength, TE total elongation, RA reduction of area

that this is due to the decrease in both activity and diffusivity of C by Al additions. And Lee et al. [53]

reported that Al addition to Fe–Mn–C TWIP steels reduces the DSA effect since DSA is the result of an

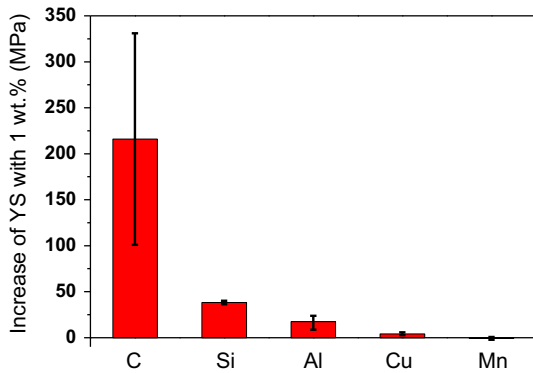


Figure 3 Effect of alloy elements on increase in YS with increasing one weight percent.

interaction of C–Mn point complexes and stacking faults in TWIP steels. Interestingly, the 0.3C steel having a chemical composition of Fe–20Mn–0.3C–1.03Al did not show serrations, which means the critical ratio of Al to C to eliminate the serration flow in the tensile curve was in existence. Figure 5a, b provides the critical strain and stress for the onset of serration with the ratio of Al to C based on the present results and published studies [25, 40, 53, 54]. The

critical strain and stress for the onset of serration were increased with increasing the ratio of Al to C although some deviations were in existent due to the different Mn contents, grain size, and various strain rates of 10^{-4} – 10^{-3} s $^{-1}$. The serrated flow was not observed when the ratio of Al to C is over about 3.0, e.g., 3.3 in the 2Al and 0.3C steels, and 4.3 in the 3.0Al steel. Also, other TWIP steels in the studies did not have serrations when the ratio of Al to C is over about 3.0. From both scientific and industrial point of view, this result is beneficial to design chemical compositions because DSA-assisted strain marks on the surface of products by inhomogeneous deformation as well as crack formation have been reported in Fe–Mn–C TWIP steels during plastic deformation [23, 55–59]. Meanwhile, Fig. 5c and d represents the critical strain and stress for the onset of serration with the ratio of Cu to C based on the present results and published studies [16, 26, 49], which showed that Cu also reduced the activation of serration, but the effect is very small compared to the Al additions. Overall, it was clearly observed that serration was decreased with increasing Cu, Mn, Si, and Al contents, and

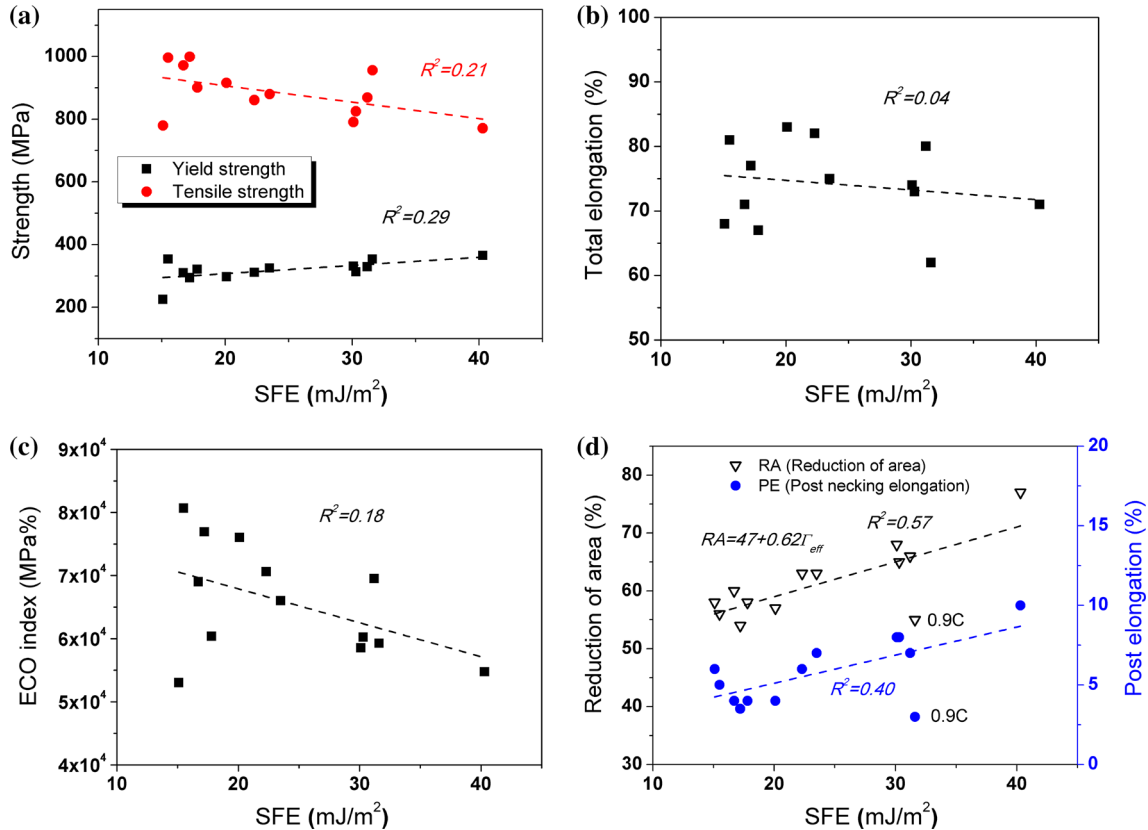


Figure 4 Variations in tensile properties of a strength, b TE, c ECO index, and d RA and PE with SFE of the 13 steels.

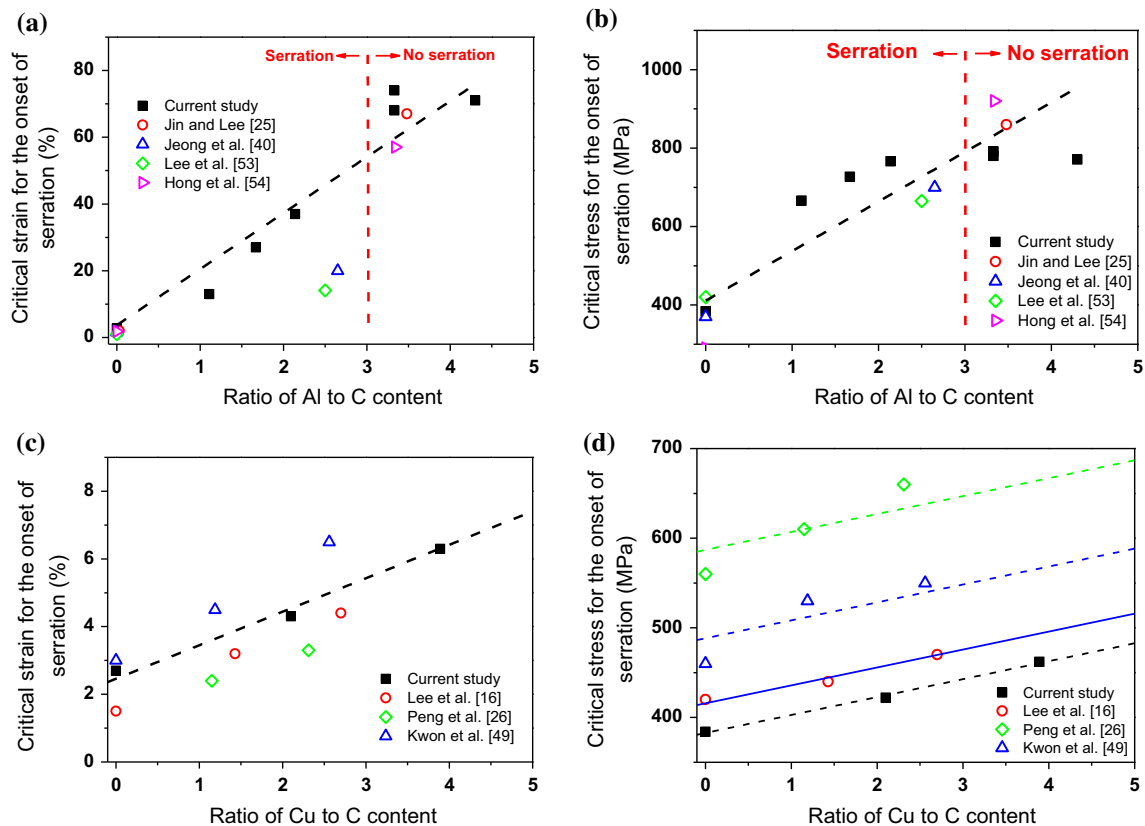


Figure 5 Critical strain and stress for the onset of serration with the ratio of **a, b** Al to C content and **c, d** Cu to C content.

decreasing C content. This implies that the reduction of TS or strain hardening rate with increasing Cu, Mn, and Al contents and decreasing C content was attributed to the occurrence of DSA as well as the generation of deformation twins during plastic deformation [33]. For instance, 3.0Al, 2Al, and 0.3C steels exhibited relatively low TS and TE due to the no DSA effect and suppression of deformation twinning. It should be noted that these results were derived at the strain rate of 10^{-4} – 10^{-3} s $^{-1}$. Accordingly, further research is necessary at high strain rate level since DSA is strongly dependent on the strain rate and temperature.

Figure 6a shows the variation in PE as a function of critical strain for the onset of serration of the 13 steels. The PE increased with increasing the critical strain for the onset of serration, which means PE depends on the DSA behaviors. Several studies [55–58] reported that necking behavior in TWIP steels is dependent on the strain rate, temperature, and C content since these factors control the occurrence of DSA. Yang et al. [55] reported that DSA effect brings the PLC band in Fe–Mn–C TWIP steel during the

tensile test, where strain localization and stress concentration occur, resulting in a shear fracture without obvious necking. Yu et al. [57] reported DSA-assisted crack formation along the grain boundary junctions and deformation twin boundaries within edge and side surface of specimen during the tensile test in Fe–Mn–C TWIP steels. In addition, Koyama et al. [58] reported that the increase in C content promoted DSA, leading to premature fracture in TWIP steels. The premature fracture was clearly observed in the 0.9C steel as shown in Fig. 2a: a very small PE. This small PE of 0.9C steel led to smaller RA value than expected. Based on the present results and literature reviews, the author concluded that DSA induced the strain localization by PLC band, resulting in the premature fracture, finally leading to the decrease in PE in TWIP steels. And this decreased PE can contribute the reduction of RA in TWIP steels. It is worth noting that DSA behaviors were strongly related to the chemical composition as shown in Figs. 1 and 2, not the SFE [4, 51, 52]. It is widely accepted that UE mainly depends on the twinning rate [3, 5]. And PE mainly depends on the strain localization by the DSA

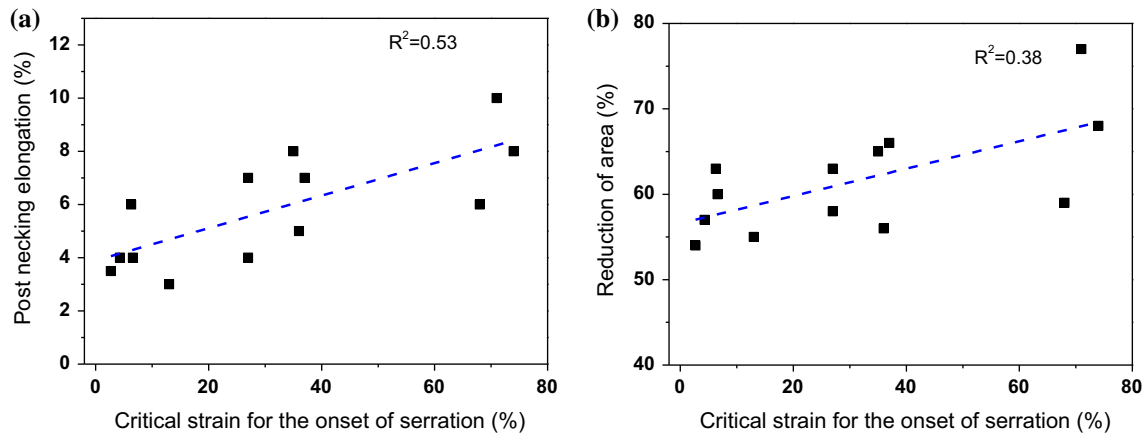


Figure 6 Variations of **a** PE and **b** RA with critical strain for the onset of serration of the 13 high-manganese steels.

in TWIP steels based on the above results. Both UE and PE have an effect on the necking geometry or RA value, which is the reason that the RA had a weak relationship with the critical strain for the onset of serration or DSA in comparison with PE as shown in Fig. 6b stemming from the partial dependence of RA on PE.

It is to be noted that RA value depends on the chemical composition since DSA behaviors are highly related to the chemical composition. TE mainly depends on the UE or twinning rate since the contribution of PE to TE is negligible in TWIP steels. In such a case, elongation itself cannot represent the influence of chemical composition. For example, Al, Cu, and Mn additions increase SFE, but generally decrease the twinning rate or UE in Fe–Mn–C TWIP steels, and finally decrease the TE, while RA value increased despite the decrease in UE because the PE increased with the addition of above alloying elements. Meanwhile, SFE may have a partial relationship with chemical composition itself since SFE can be controlled by chemical composition; however, elongation cannot reflect the influence of chemical composition, which showed no relationship between TE and SFE as shown in Fig. 4b, whereas RA value reflects both twinning behaviors and chemical composition itself. In other words, RA depends on both UE related to twinning rate and PE or necking geometry related to DSA in TWIP steels. Based on the above results, it is reasonable to conclude that RA value is a potential indicator for SFE, which means we can predict the SFE in Fe–Mn–C TWIP steels by measuring the RA value and vice versa as the

following equation although it had some deviations to predict the C effect (Fig. 4d):

$$RA (\%) = 47 + 0.62\Gamma_{\text{eff}} \left(\text{mJ/m}^2 \right). \quad (4)$$

To the best of author’s knowledge, this kind of relationship has not been reported before because most of the researchers have used plate-type tensile specimens, which is mainly due to the interest in applying TWIP steels to plate products. However, it should be noted that this empirical equation was derived only for the limited range of SFE and chemical compositions in the current study; thus, it requires further research and validation from other researchers or experiments. Meanwhile, the effect of twinning and DSA behavior on RA was qualitatively investigated in the present study. Future work will be focused on the quantitative analysis between twinning/DSA behaviors and RA based on the microstructural characterizations.

Twinning stress

The stress required to initiate a twin formation is usually termed as twinning stress. It is well known that twinning stress is one of the critical parameters to understand the twinning behaviors and it is strongly affected by SFE, temperature, and grain size/orientation. Based on the author’s experiences and the literature review, it is notoriously difficult and takes much time to determine the twinning stress experimentally in TWIP steels; thus, several researchers proposed the empirical model to predict the twinning stress. In this study, the twinning stress

was evaluated using the group 1 TWIP steels based on the EBSD techniques,

Figure 7a–e shows the inverse pole figure (IPF) maps at the strain of 0.095, and twin boundaries having a misorientation angle of $58^\circ < \theta < 62^\circ$ are also represented in Fig. 7f–j. Quarter areas on the section of samples perpendicular to the loading axis were observed. Parallel lines inside grains were twin bundles consisting of several individual thin twins [40, 44, 60]. Since the propensity for deformation twinning depends on the grain orientation, Schmid factor analysis was applied to determine the favorable and unfavorable grain orientations for twinning under tensile stress as shown in Fig. 7k–o. In this contour, Schmid factors were calculated for the leading partial dislocations of $(11\bar{1})[112]$ systems, which is the highest Schmid factors for twin under tensile stress [44, 61]. The black circles depicted in orientation triangle mean twinned grains, and the white ones present non-twinned grains.

Several grains of the 0CuAlSi steel had deformation twins (Fig. 7a, f), and a few grains had deformation twin in the 1.5Cu steel (Fig. 7b, g). However, few deformation twins were observed in the 3.0Cu and 1.5Al steels and no deformation twin appeared in

the 3.0Al steel. Meanwhile, deformation twins were occurred in the grains around $\langle 111 \rangle$ and $\langle 101 \rangle$ orientations due to the orientation dependence of deformation twinning. That is, twins appeared in the grains with higher Schmid factor for twin. The twin volume fraction was increased at the strain of 0.18 as shown in Fig. 8. Most of the grains except for $\langle 001 \rangle$ grains had deformation twins in the 0CuAlSi steel (Fig. 8a, f, k), whereas a few deformation twins were observed in the 3.0Al steel, whose behavior is highly related to SFE and grain orientations. The twin density of the 3.0Cu steel was similar to that of the 1.5Al steel. In addition, the grain rotation was clearly observed in all the steels at this strain.

As shown in Fig. 9a, the relative twin volume fraction was measured as a function of true stress using the EBSD techniques to have quantitative information on the twinning behaviors. The high-angle boundary having misorientation angle of $58^\circ < \theta < 62^\circ$ was selected, and the total length of this value was divided by the total measured area, μm^{-1} . Annealing twins were excluded from this calculation. The twin volume fraction progressively increased with stress at all the steels, but the difference of twin volume fraction among steels was

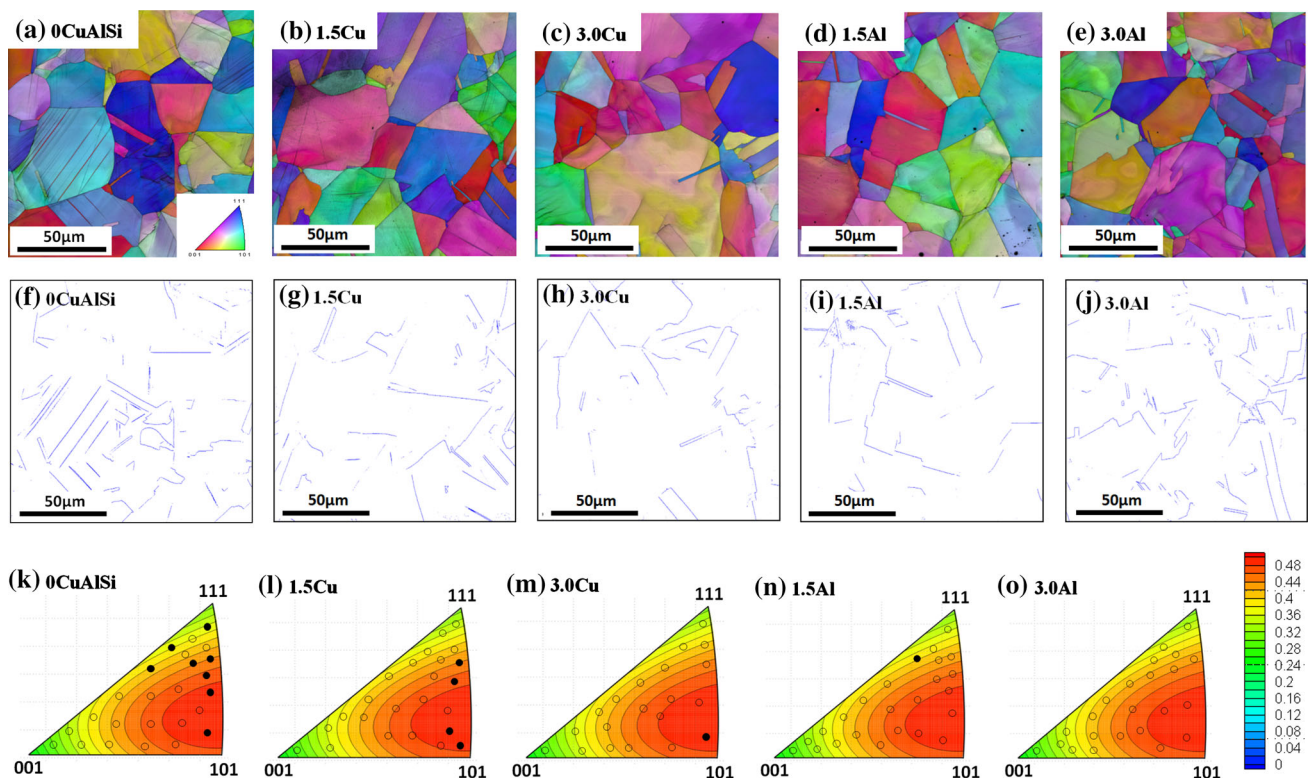


Figure 7 Comparison of a–e IPF, f–j twin boundary maps, and k–o Schmid factor analysis at the strain of 0.095.

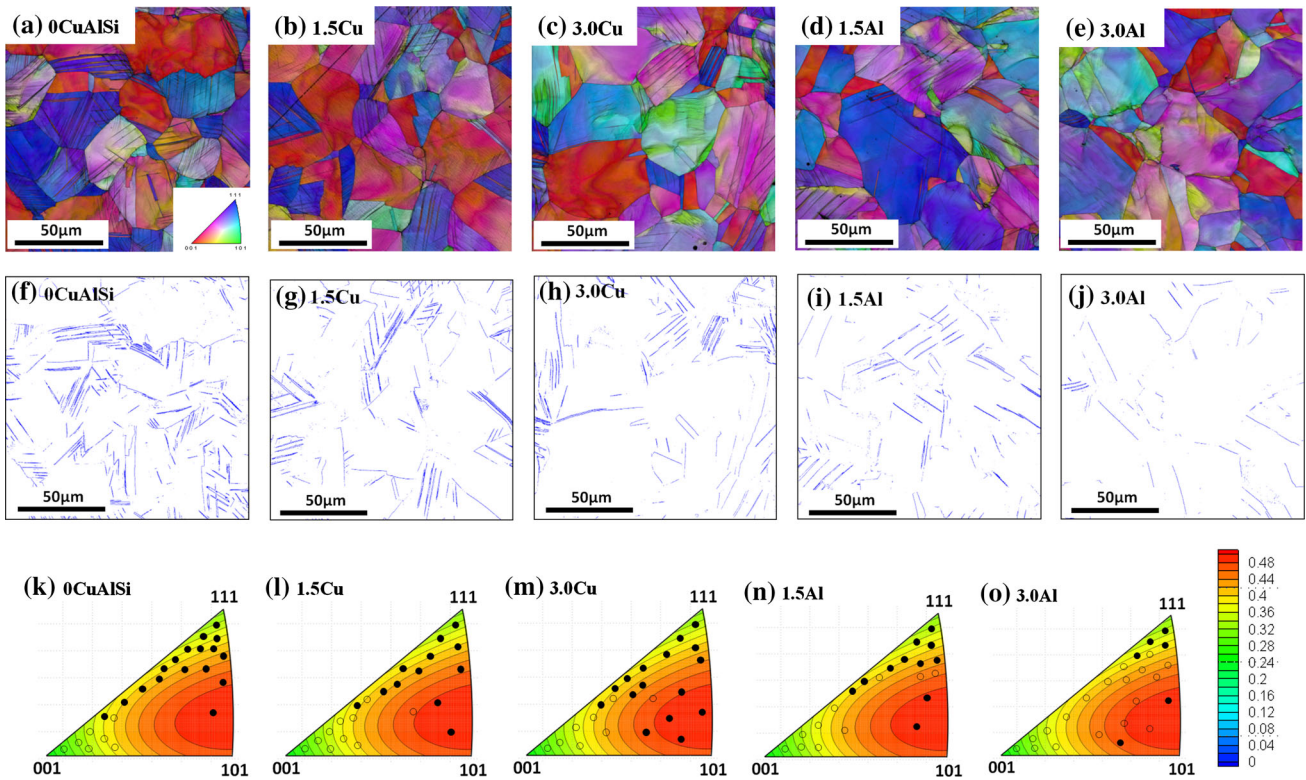


Figure 8 Comparison of a–e IPF, f–j twin boundary maps, and k–o Schmid factor analysis at the strain of 0.18.

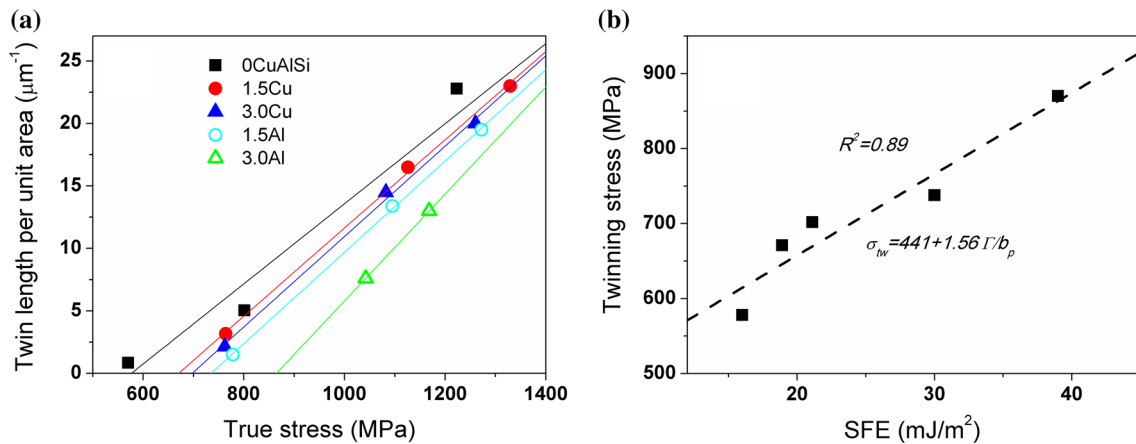


Figure 9 a Comparison of variations in length per unit area of deformation twin with true stress and b variations in twinning stress as a function of SFE.

clearly observed. A significant increase in twin volume fraction was observed in the 0CuAlSi steel, which means deformation twinning was significantly activated at lower stress compared to the other steels, whereas the 3.0Al steel showed lower twin volume fraction with increasing stress. Extrapolation of linear fitting curves to the *x*-axis can provide a minimum stress required to the generation of deformation twin in the steels, which is displayed in Fig. 9b. This

figure shows that the stress (σ_{tw}) for the twin activation increased with increasing the SFE and σ_{tw} had a linear relationship with SFE as given in Eq. (5), indicating that twinning behavior is strongly affected by SFE in high-manganese steels.

$$\sigma_{tw} = 441 + 1.56 \frac{\Gamma}{b_p}$$

$$R^2 = 0.89, \tag{5}$$

where b_p is the Burgers vector of partial dislocation and it is about 0.144 nm in these steels [50].

In addition, twinning stress can be estimated using the curve of strain hardening rate as shown in Fig. 10. Empirically, strain hardening rate curve was sharply dropped at the initial stage and then it was flattened and/or increased with the help of planar dislocations and deformation twinning in TWIP steels [3, 5], which means the transition point of curve was highly related to the twinning stress in steels deformed by twinning mechanism. The transition point was drawn as arrows in Fig. 10b. The transition strain was increased with SFE: The 0CuAlSi steel had the lowest transient strain and corresponding stress, and the 3Al steel had the highest values. The 3.0Cu and the 1.5Al had similar values, which is consistent with the results from microstructural evolution. Figure 10c compares the twinning stress evaluated from the strain hardening rate curve with the twinning stress measured from EBSD twin length calculation (Fig. 9), indicating that the twinning stress calculated by

EBSD techniques in the current study was reliable to use despite the limited number of specimens. Inversely, we could roughly estimate the twinning stress by tensile curves.

Meanwhile, several models have been proposed in FCC structures as a function of SFE, grain size, and grain orientation to predict twinning stress. The main idea of those models is the dissociation of the perfect dislocation when it glides on $\langle 111 \rangle$ planes since the dissociated partial dislocations are believed to be the embryos for deformation twinning. It is accepted that the activation of multiple slip and occurrence of dislocation pileup are required to nucleate deformation twins, which means a certain amount of deformation by multiple slip is necessary. Twinning stress is highly related to the above amount of multiple slip before twinning, and it depends on the SFE, grain size, and grain orientation of materials.

The calculation of critical stress for onset of stacking faults (τ_{sf}) is necessary in order to calculate σ_{tw} in present high-manganese steels, because stacking

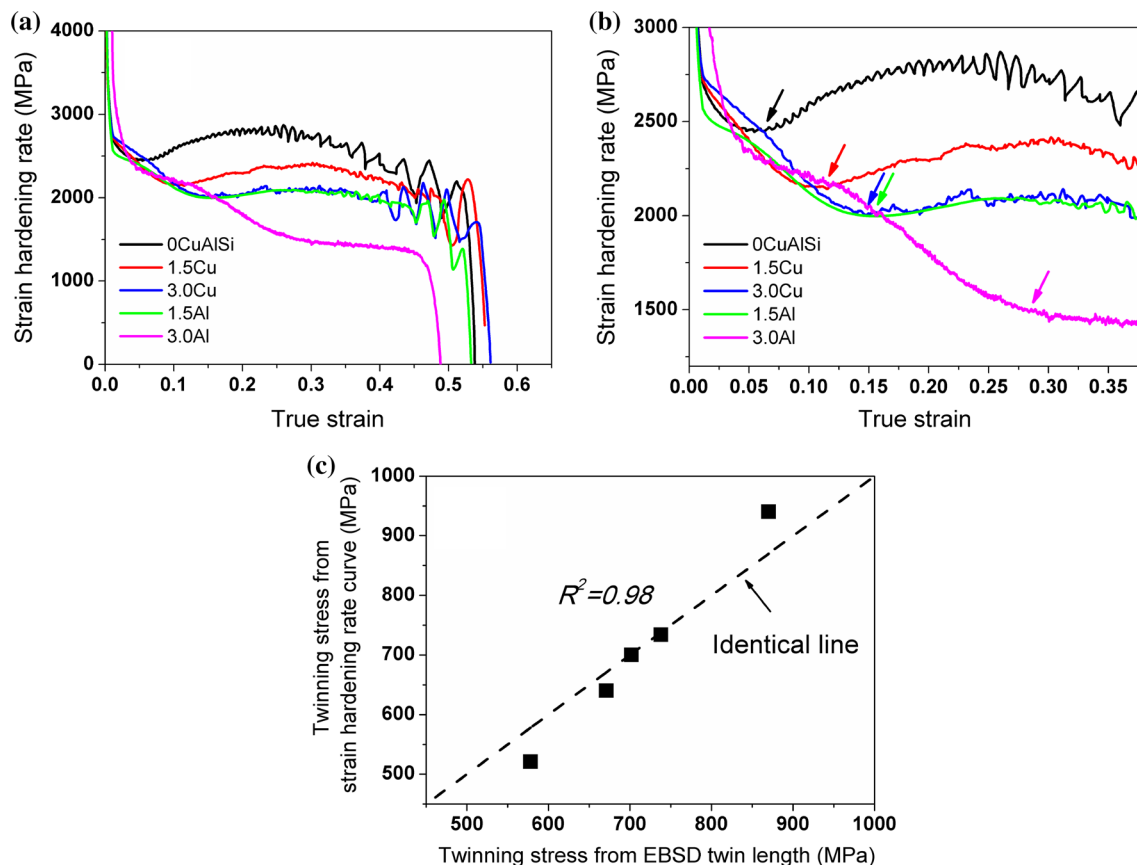


Figure 10 Comparison of **a** strain hardening curves, **b** enlarged strain hardening curves to estimate the twinning stress, and **c** twinning stress calculated from EBSD twin length measurement and evaluated from the strain hardening rate curve in the five steels.

faults are generally considered as a precursor of deformation twin. τ_{sf} is defined as the required separation stress between leading partial dislocation and its trailing partial dislocation and calculated as the following equation [62]:

$$\tau_{sf} = \frac{\Gamma}{b}, \quad (6)$$

where b is the Burgers vector of perfect dislocation. The critical shear twinning stress (τ_{tw}) is the required stress that makes an infinite separation distance between leading partial and its trailing partial, and calculated as follows [63]:

$$\tau_{tw} = \frac{2\Gamma}{b_p}. \quad (7)$$

According to Figs. 7 and 8, twinning stress was strongly dependent on the grain orientation. The influence of grain orientation was taken into consideration to make a relationship between τ_{tw} and σ_{tw} via Schmid factor. The selection of Schmid factor 0.5 is reasonable in polycrystalline metals since deformation twins appeared in the grains at the highest Schmid factor as shown in Figs. 7 and 8; therefore, σ_{tw} is calculated as the following equation:

$$\sigma_{tw} = \frac{4\Gamma}{b_p}. \quad (8)$$

This equation was similar to the Byun's model [63] except for the applied Schmid factor. Byun chose 0.326 as a Schmid factor for calculating twinning stress, while 0.5 was selected as a Schmid factor in the present study. Table 3 summarizes the published models for predicting the twinning stress in FCC structures. Although all the equations have different forms, the main results are the same: Twinning stress decreased with decreasing SFE and increasing grain size. In other words, deformation twinning was activated earlier at the low strain or stress with decreasing SFE and increasing grain size.

Figure 11 shows the comparison of the experimental twinning stresses in the present study (Fig. 9b) and the calculated twinning stresses (Table 3) as a function of SFE. The twinning stress by Byun's model was much higher than the measured twinning stress since Byun developed this model for single crystal. In contrast, the present model relatively well predicted the twinning stress. Based on Figs. 7 and 8, most of the grains with higher Schmid factor initially had deformation twins, indicating that Schmid factor of

0.5 was needed to calculate the twinning stress in polycrystalline metals. The predicted model had a higher slope compared to the experimental data since this model did not consider the grain size effect. Most of the prediction models for polycrystalline metals had a lower slope in comparison with the models for single-crystalline metals. Meanwhile, the twinning stress predicted by Gutierrez-Urrutia et al.'s model [62] was lower than the experimental data, but the slope had a good agreement with the experiments. The Mahato et al.'s model [64] relatively well predicted the twinning stress. Among the proposed models, Steinmetz et al.'s model [65] well predicted the twinning stress compared to the present experiment. This model was developed based on the twin embryo mechanism proposed by Mahajan and Chin [66] to explain the nucleation of deformation twin. Also, Lee et al.'s modified model [39] of Steinmetz et al.'s in order to consider grain size effect well predicted the twinning stress. Overall, the author can deduce the following results based on the comparative study between measured data and earlier proposed model for twinning stress.

1. Twinning stress had a strong relationship with SFE in high-manganese steels: linear relationship.
2. Schmid factor of 0.5 was needed to use for polycrystalline metals to evaluate the twinning stress using the models based on the single crystal.
3. We needed to consider the grain size effect to predict the twinning stress accurately in polycrystalline metals.

Conclusions

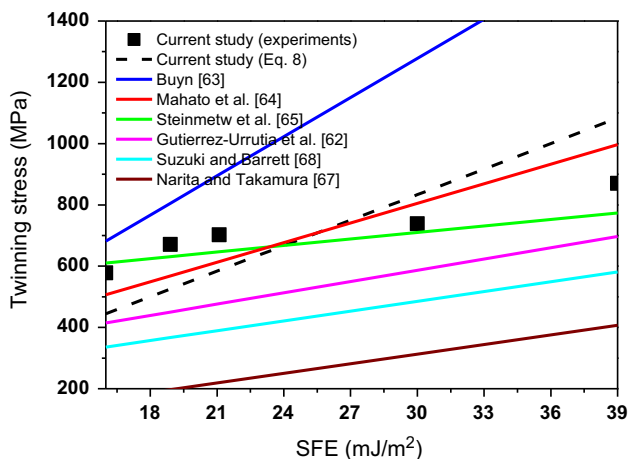
Based on the systemic study on the influence of SFE and chemical compositions on tensile properties using the 14 Fe–Mn–C high-manganese steels, the following conclusions were drawn:

1. Cu and Al played similar roles in TWIP steels: increase in SFE, YS, and RA and decrease in TS and serration. However, the effect of Al content was stronger than that of Cu content. Addition of C content highly increased the YS, but excessive C addition led to the premature fracture, i.e., small PE and RA. In Fe–Mn–C TWIP steel, Si had to be carefully added since excessive Si addition

Table 3 Published prediction models for the twinning stress in FCC structures

Proposed researchers	Materials	Considering grain size	Twinning stress (shear stress, τ_{tw})
Byun [63]	Stainless steel	No	$\tau_{tw} = \frac{2\Gamma}{b_p}$
Gutierrez-Urrutia et al. [62]	TWIP steel	Yes	$\tau_{tw} = \frac{\Gamma}{b} + \frac{K_{tw}}{\sqrt{D}}$
Narita and Takamura [67]	Silver and copper alloys	No	$\tau_{tw} = \frac{\Gamma}{2b_p}$
Steinmetz et al. [65]	TWIP steel	No	$\tau_{tw} = \frac{\Gamma}{3b_p} + \frac{3Gb_p}{L_0}$
Suzuki and Barrett [68]	Silver and gold alloys	No	$\tau_{tw} = \frac{\Gamma}{2b_p} + \frac{Gb_p}{L_0}$
Meyer et al. [69]	Copper alloys	Yes	$\tau_{tw} = \frac{\Gamma}{b_p} + \frac{K_{\tau}}{\sqrt{D}}$
Mahato et al. [64]	TWIP steel	No	$\tau_{tw} = \frac{\Gamma}{b_p} + \frac{Gb_p}{L_0}$
Lee et al. [39]	TWIP steel	Yes	$\tau_{tw} = \frac{\Gamma_{eff}}{3b_p} + \frac{3Gb_p}{L_0}$

b_p , burgers vector of partial dislocation; b , burgers vector of perfect dislocation; G , shear modulus; D , grain size; Γ , stacking fault energy; Γ_{eff} , effective stacking fault energy; K_{tw} , Hall–Petch constant; L_0 , width of twin embryo; K , numerical constant

**Figure 11** Comparison of experimental and calculated twinning stress as a function of SFE.

resulted in early fracture due to the decrease in SFE.

- The critical ratio of Al to C to eliminate the serration flow in high-manganese steels was in existence: The serration flow in tensile curve was not observed when the ratio of Al to C is over about 3.0.
- DSA or PLC decreased the PE during the tensile test associated with the premature fracture, leading to the reduction of RA in TWIP steels.
- The RA had a linear relationship with SFE, which means that RA is a potential indicator to predict SFE in high-manganese steels.
- Twinning stress had a linear relationship with SFE in high-manganese steels, and Schmid factor

of 0.5 was needed to use for polycrystalline metals to evaluate the twinning stress using the models based on the single crystal.

Acknowledgements

This research was supported by the Tongmyong University Research Grants 2019 (2019A005).

References

- Bouaziz O, Allain S, Scott CP, Cugy P, Barbier D (2011) High manganese austenitic twinning induced plasticity steels: a review of the microstructure properties relationships. *Curr Opin Solid State Mater Sci* 15:141–168
- Grassel O, Kruger L, Frommeyer G, Meyer LW (2000) High strength Fe–Mn–(Al, Si) TRIP/TWIP steels development-properties-application. *Int J Plast* 16:1391–1409
- Barbier D, Gey N, Allain S, Bozzolo N, Humbert M (2009) Analysis of the tensile behavior of a TWIP steel based on the texture and microstructure evolutions. *Mater Sci Eng A* 500:196–206
- Dastur YN, Leslie WC (1981) Mechanism of work hardening in Hadfield manganese steel. *Metall Trans A* 12:749–759
- Jin JE, Lee YK (2009) Strain hardening behavior of a Fe–18Mn–0.6C–1.5Al TWIP steel. *Mater Sci Eng A* 527:157–161
- De Cooman BC, Estrin Y, Kim SK (2018) Twinning-induced plasticity (TWIP) steels. *Acta Mater* 142:283–362

- [7] Zambrano OA (2018) A general perspective of Fe–Mn–Al–C steels. *J Mater Sci* 53:14003–14062. <https://doi.org/10.1007/s10853-018-2551-6>
- [8] Allain S, Chateau JP, Bouaziz O, Migot S, Guelton N (2004) Correlations between the calculated stacking fault energy and the plasticity mechanisms in Fe–Mn–C alloys. *Mater Sci Eng A* 387–389:158–162
- [9] Saeed-Akbari A, Imlau J, Prahll U, Bleck W (2009) Derivation and variation in composition-dependent stacking fault energy maps based on subregular solution model in high-manganese steels. *Metall Mater Trans A* 40:3076–3090
- [10] Kim JK, De Cooman BC (2016) Stacking fault energy and deformation mechanisms in Fe–xMn–0.6C–yAl TWIP steel. *Mater Sci Eng A* 676:216–231
- [11] Curtze S, Kuokkala VT (2010) Dependence of tensile deformation behavior of TWIP steels on stacking fault energy, temperature and strain rate. *Acta Mater* 58:5129–5141
- [12] Park KT, Kim G, Kim SK, Lee SW, Hwang SW, Lee CS (2010) On the transitions of deformation modes of fully austenitic steels at room temperature. *Met Mater Int* 16:1–6
- [13] Remy L (1997) Temperature variation of the intrinsic stacking fault energy of a high manganese austenitic steel. *Acta Mater* 25:173–179
- [14] Dumay A, Chateau JP, Allain S, Migot S, Bouaziz O (2008) Influence of addition elements on the stacking-fault energy and mechanical properties of an austenite Fe–Mn–C steel. *Mater Sci Eng A* 483–484:184–187
- [15] Park KT, Jin KG, Han SH, Hwang SW, Choi K, Lee CS (2010) Stacking fault energy and plastic deformation of fully austenitic high manganese steels: effect of Al addition. *Mater Sci Eng A* 527:3651–3661
- [16] Lee S, Kim J, Lee SJ, De Cooman BC (2011) Effect of Cu addition on the mechanical behavior of austenitic twinning-induced plasticity steel. *Scr Mater* 65:1073–1076
- [17] Zambrano OA (2016) Stacking fault energy maps of Fe–Mn–Al–C–Si steels: effect of temperature, grain size, and variations in compositions. *J Eng Mater Technol*. <https://doi.org/10.1115/1.4033632>
- [18] Kim JK, Estrin Y, Beladi H, Timokhina L, Chin KG, Kim SK, De Cooman BC (2012) Constitutive modeling of the tensile behavior of Al-TWIP steel. *Metall Mater Trans A* 43A:479–490
- [19] Koyama M, Sawaguchi T, Lee T, Lee CS, Tsuzaki K (2011) Work hardening associated with ϵ -martensitic transformation, deformation twinning and dynamic strain aging in Fe–17Mn–0.6C and Fe–17Mn–0.8C TWIP steels. *Mater Sci Eng A* 528:7310–7316
- [20] Shun T, Wan CM, Byrne JG (1992) A study of work hardening in austenitic Fe–Mn–C and Fe–Mn–Al–C alloys. *Acta Metall Mater* 40:3407–3412
- [21] Zhou P, Huang MX (2015) On the mechanisms of different work-hardening stages in twinning-induced plasticity steels. *Metall Mater Trans A* 46:5080–5090
- [22] Lee SY, Lee SI, Hwang B (2018) Effect of strain rate on tensile and serration behaviors of an austenitic Fe–22Mn–0.7C twinning-induced plasticity steel. *Mater Sci Eng A* 711:22–28
- [23] Chin KG, Kang CY, Shin SY, Hong S, Lee S, Kim HS, Kim K, Kim NJ (2011) Effects of Al addition on deformation and fracture mechanisms in two high manganese TWIP steels. *Mater Sci Eng A* 528:2922–2928
- [24] Jung YS, Kang S, Jeong K, Jung JG, Lee YK (2013) The effects of N on the microstructures and tensile properties of Fe–15Mn–0.6C–2Cr–xN twinning-induced plasticity steels. *Acta Mater* 61:6541–6548
- [25] Jin JE, Lee YK (2012) Effect of Al on microstructure and tensile properties of C-bearing high Mn TWIP steel. *Acta Mater* 60:1680–1688
- [26] Peng X, Zhu D, Hu Z, Yi W, Liu H, Wang M (2013) Stacking fault energy and tensile deformation behavior of high-carbon twinning-induced plasticity steels: effect of Cu addition. *Mater Des* 45:518–523
- [27] Xiong R, Peng H, Wang S, Si H, Wen Y (2015) Effect of stacking fault energy on work hardening behaviors in Fe–Mn–Si–C high manganese steels by varying silicon and carbon contents. *Mater Des* 85:707–714
- [28] Hong S, Shin SY, Kim HS, Lee S, Kim S, Chin KG, Kim NJ (2012) Effects of aluminum addition on tensile and cup forming properties of three twinning induced plasticity steels. *Metall Mater Trans A* 43A:1870–1883
- [29] Yang HK, Zhang ZJ, Zhang ZF (2013) Comparison of work hardening and deformation twinning evolution in Fe–22Mn–0.6C–(1.5Al) twinning-induced plasticity steels. *Scr Mater* 68:992–995
- [30] Lee S, Kim J, Lee SJ, De Cooman BC (2011) Effect of nitrogen on the critical strain for dynamic strain aging in high-manganese twinning-induced plasticity steel. *Scr Mater* 65:528–531
- [31] Yang HK, Tian YZ, Zhang ZJ, Zhang ZF (2018) Simultaneously improving the strength and ductility of Fe–22Mn–0.6C twinning-induced plasticity steel via nitrogen addition. *Mater Sci Eng A* 715:276–280
- [32] Lee SJ, Jung YS, Baik SI, Kim YW, Kang M, Woo W, Lee YK (2014) The effect of nitrogen on the stacking fault energy in Fe–15Mn–2Cr–0.6C–xN twinning-induced plasticity steels. *Scr Mater* 92:23–26

- [33] Liu S, Qian L, Meng J, Ma P, Zhang F (2015) On the more persistently-enhanced strain hardening in carbon-increased Fe–Mn–C twinning-induced plasticity steel. *Mater Sci Eng A* 639:425–430
- [34] Torganchuk V, Belyakov A, Kaibyshev R (2017) Effect of rolling temperature on microstructure and mechanical properties of 18%Mn TWIP/TRIP steels. *Mater Sci Eng A* 708:110–117
- [35] Zambrano OA, Valdes J, Aguilar Y, Coronado JJ, Rodriguez SA, Loge RE (2017) Hot deformation of a Fe–Mn–Al–C steel susceptible of k-carbide precipitation. *Mater Sci Eng A* 689:269–285
- [36] Liu FC, Yang ZN, Zheng CL, Zhang FC (2012) Simultaneously improving the strength and ductility of coarse-grained Hadfield steel with increasing strain rate. *Scr Mater* 66:431–434
- [37] Lee T, Koyama M, Tsuzaki K, Lee YH, Lee CS (2012) Tensile deformation behavior of Fe–Mn–C TWIP steel with ultrafine elongated grain structure. *Mater Lett* 75:169–171
- [38] Hwang JK (2018) Effects of caliber rolling on microstructure and mechanical properties in twinning-induced plasticity (TWIP) steel. *Mater Sci Eng A* 711:156–164
- [39] Lee SM, Lee SJ, Lee S, Nam JH, Lee YK (2018) Tensile properties and deformation mode of Si-added Fe–18Mn–0.6C steels. *Acta Mater* 144:738–747
- [40] Jeong K, Jin JE, Jung YS, Kang S, Lee YK (2013) The effects of Si on the mechanical twinning and strain hardening of Fe–18Mn–0.6C twinning-induced plasticity steel. *Acta Mater* 61:3399–3410
- [41] Kusakin P, Belyakov A, Molodov DA, Kaibyshev R (2017) On the effect of chemical composition on yield strength of TWIP steels. *Mater Sci Eng A* 687:82–84
- [42] Gwon H, Kim JK, Shin S, Cho L, De Cooman BC (2017) The effect of vanadium micro-alloying on the microstructure and the tensile behavior of TWIP steel. *Mater Sci Eng A* 696:416–428
- [43] Hwang JK (2018) Effect of copper and aluminum contents on wire drawing behavior in twinning-induced plasticity steels. *Mater Sci Eng A* 737:188–197
- [44] Hwang JK, Yi IC, Son IH, Yoo JY, Kim B, Zargaran A, Kim NJ (2015) Microstructural evolution and deformation behavior of twinning-induced plasticity (TWIP) steel during wire drawing. *Mater Sci Eng A* 644:41–52
- [45] Olson GB, Cohen M (1976) A general mechanism of martensitic nucleation: part I. General concepts and the FCC \rightarrow HCP transformation. *Metall Trans A* 7:1897–1904
- [46] Adler PH, Olson GB, Owen WS (1986) Strain hardening of Hadfield manganese steel. *Metall Trans A* 17:1725–1737
- [47] Lee YK, Choi C (2000) Driving force for $\gamma \rightarrow \epsilon$ martensitic transformation and stacking fault energy of γ in Fe–Mn binary system. *Metall Mater Trans A* 31:355–360
- [48] Dieudonne T, Marchetti L, Wery M, Chene J, Allely C, Cugy P, Scott CP (2014) Role of copper and aluminum additions on the hydrogen embrittlement susceptibility of austenitic Fe–Mn–C TWIP steels. *Corros Sci* 82:218–226
- [49] Kwon YJ, Lee T, Lee J, Chun YS, Lee CS (2015) Role of Cu on hydrogen embrittlement behavior in Fe–Mn–C–Cu TWIP steel. *Int J Hydrog Energy* 40:7409–7419
- [50] Ghasri-Khouzani M, McDermid JR (2015) Effect of carbon content on the mechanical properties and microstructure evolution of Fe–22Mn–C steels. *Mater Sci Eng A* 621:118–127
- [51] Chen L, Kim HS, Kim SK, DeCooman BC (2007) Localized deformation due to Portevin–LeChatelier effect in 18Mn–0.6C TWIP austenitic steel. *ISIJ Int* 47:1804–1812
- [52] Qian L, Guo P, Zhang F, Meng J, Zhang M (2013) Abnormal room temperature serrated flow and strain rate dependence of critical strain of a Fe–Mn–C twin-induced plasticity steel. *Mater Sci Eng A* 561:266–269
- [53] Lee SJ, Kim J, Kane SN, De Cooman BC (2011) On the origin of dynamic strain aging in twinning-induced plasticity steels. *Acta Mater* 59:6809–6819
- [54] Hong S, Shin SY, Lee J, Ahn DH, Kim HS, Kim SK, Chin KG, Lee S (2014) Serration phenomena occurring during tensile tests of three high-manganese twinning-induced plasticity (TWIP) steels. *Metall Mater Trans A* 45A:633–646
- [55] Yang HK, Tian YZ, Zhang ZJ, Yang CL, Zhang P, Zhang ZF (2017) Tensile fracture modes in Fe–22Mn–0.6C and Fe–30Mn–3Si–3Al twinning-induced plasticity (TWIP) steels. *Metall Mater Trans A* 48:4458–4462
- [56] Yang CL, Zhang ZJ, Zhang P, Zhang ZF (2017) The premature necking of twinning-induced plasticity steels. *Acta Mater* 136:1–10
- [57] Yu HY, Lee SM, Nam JH, Lee SJ, Fabregue D, Park MH, Tsuji N, Lee YK (2017) Post-uniform elongation and tensile fracture mechanisms of Fe–18Mn–0.6C–xAl twinning-induced plasticity steels. *Acta Mater* 131:435–444
- [58] Koyama M, Shimomura Y, Chiba A, Akiyama E, Tsuzaki K (2017) Room-temperature blue brittleness of Fe–Mn–C austenitic steels. *Scr Mater* 141:20–23
- [59] Kim JG, Hong S, Anjabin N, Park BH, Kim SK, Chin KG, Lee S, Kim HS (2015) Dynamic strain aging of twinning-induced plasticity (TWIP) steel in tensile testing and deep drawing. *Mater Sci Eng A* 633:136–143
- [60] Soulami A, Choi KS, Shen YF, Liu WN, Sun X, Khaleel MA (2011) On deformation twinning in a 17.5% Mn-TWIP steel: a physically based phenomenological model. *Mater Sci Eng A* 528:1402–1408

- [61] Karaman I, Sehitoglu H, Gall K, Chumlyakov YI, Maier HJ (2000) Deformation of single crystal Hadfield steel by twinning and slip. *Acta Mater* 48:1345–1359
- [62] Gutierrez-Urrutia I, Zaefferer S, Raabe D (2010) The effect of grain size and grain orientation on deformation twinning in a Fe–22Mn–0.6C TWIP steel. *Mater Sci Eng A* 527:3552–3560
- [63] Byun TS (2003) On the stress dependence of partial dislocation separation and deformation microstructure in austenitic stainless steels. *Acta Mater* 51:3063–3071
- [64] Mahato B, Shee SK, Sahu T, Chowdhury SG, Sahu P, Porter DA, Karjalainen LP (2015) An effective stacking fault energy viewpoint on the formation of extended defects and their contribution to strain hardening in Fe–Mn–Si–Al twinning-induced plasticity steel. *Acta Mater* 86:69–79
- [65] Steinmetz DR, Japel T, Wietbrock B, Eisenlohr P, Gutierrez-Urrutia I, Saeed-Akbari A, Hickel T, Roters F, Raabe D (2013) Revealing the strain-hardening behavior of twinning-induced plasticity steels: theory, simulation, experiments. *Acta Mater* 61:494–510
- [66] Mahajan S, Chin GY (1973) Formation of deformation twins in fcc crystals. *Acta Metall* 21:1353–1363
- [67] Narita N, Takamura J (1974) Deformation twinning in silver and copper alloy crystals. *Philos Mag* 29:1001–1028
- [68] Suzuki H, Barrett C (1958) Deformation twinning in silver–gold alloys. *Acta Metall* 6:156–165
- [69] Mayers MA, Vohringer O, Lubarda VM (2001) The onset of twinning in metals: a constitutive description. *Acta Mater* 49:4025–4039

Publisher's Note Springer Nature remains neutral with regard to jurisdictional claims in published maps and institutional affiliations.